High bias anomaly in $YBa_2Cu_3O_{7-x}/LaMnO_{3+\delta}/YBa_2Cu_3O_{7-x}$ superconductor/ferromagnetic insulator/superconductor junctions: Evidence for a long-range superconducting proximity effect through the conduction band of a ferromagnetic insulator

T. Golod, A. Rydh, and V. M. Krasnov*
Department of Physics, Stockholm University, AlbaNova University Center, SE-10691 Stockholm, Sweden

I. Marozau, M. A. Uribe-Laverde, D. K. Satapathy,† Th. Wagner, and C. Bernhard
University of Fribourg, Department of Physics and Fribourg Centre for Nanomaterials, Chemin du Musée 3, CH-1700 Fribourg, Switzerland

We study the perpendicular transport characteristics of small superconductor/ferromagnetic insulator/superconductor ($YBa_2Cu_3O_{7-x}/LaMnO_{3+\delta}/YBa_2Cu_3O_{7-x}$) tunnel junctions. At a large bias voltage $V \sim 1$ V we observe a steplike onset of excess current that occurs below the superconducting transition temperature $T < T_c$ and is easily suppressed by a magnetic field. The phenomenon is attributed to a different type of the superconducting proximity effect of nonequilibrium electrons injected into the conduction band of the ferromagnetic insulator via a Fowler-Nordheim tunneling process. The occurrence of a strongly nonequilibrium population is confirmed by the detection of photon emission at large bias voltage. Since the conduction band in our ferromagnetic insulator is strongly spin polarized, the long range (20 nm) of the observed proximity effect provides evidence for an unconventional spin-triplet superconducting state.

I. INTRODUCTION

The manganite perovskite $La_{2-x}(Ca,Sr)_xMnO_3$ exhibits a rich phase diagram of unusual electronic and magnetic properties. Most prominent is the so-called colossal magnetoresistance (CMR) effect which occurs at $0.15 < x < 0.5$ in the context of a transition from a paramagnetic and insulating or poorly conducting state to a ferromagnetic and half-metallic state.[1,2] At somewhat lower doping at $0.1 < x < 0.15$, the corresponding transition leads into a ferromagnetic insulating (FI) state which is a consequence of charge localization below the spin-polaron mobility edge and orbital ordering at low T.[3–6] This FI state can also be achieved in off stoichiometric $LaMnO_{3+\delta}$ in which the hole doping is due to La or Mn vacancies. While half-metallic manganites are considered as promising spin polarizers,[7] the FI manganite can be an ideal spin-filter material for use in tunnel barriers with low leakage currents. Efficient spin filters are in demand for spintronic applications.[8] Spin polarization depends on many parameters, including the density of states (DOS) of electronic bands,[7,9–12] orbital hybridization, and various material issues at interfaces and on the bias voltage.[13] Metallic ferromagnets provide only modest spin polarization because both majority (↑) and minority (↓) spin bands are crossing the Fermi level E_F.[14] This problem is obviated in insulating and half-metallic ferromagnets with separated majority and minority bands at E_F, which, therefore, can facilitate an almost complete spin polarization.[8,13–15]

The antagonism between superconductivity (S) and ferromagnetism (F) leads to a variety of novel effects in hybrid S/F heterostructures,[16,17] such as the stabilization of unconventional spin-triplet superconductivity,[17,18] or the realization of π-Josephson junctions,[19] that are interesting both from fundamental and applied points of view. Electrons in a material, in contact with a superconductor, inherit phase coherence from the S side, a phenomenon known as the superconducting proximity effect. In clean normal metals (N) the proximity effect can extend over a length scale on the order of micrometers. In ferromagnetic metals the range depends on the superconducting pairing symmetry:[17,18] The conventional spin-singlet pairing is rapidly suppressed by the magnetic exchange field at a scale of ~1 nm,[16] but the unconventional spin-triplet pairing is immune to the magnetic exchange field and the range is similar as in nonmagnetic metals. Therefore long-range superconducting proximity effects, observed in ferromagnetic metals[20–22] and half metals,[23–27] are taken as evidence for a spin-triplet superconducting state induced via spin-active S/F interfaces.[17,18]

S/FI/S tunnel junctions are characterized by a nontrivial phase dynamics[17,28,29] that is useful for phase-coherent quantum spintronic devices.[15,28] Atomically thin FI layers enable sizable and almost fully spin-polarized tunnel currents that are beneficial for spintronic applications.[8,13] However, the superconducting wave function and the tunneling probability decay exponentially at an atomic scale with increasing FI thickness.[28] Thus, nanometer-thick insulators are impenetrable for electrons due to the band gap at the Fermi level E_F. Therefore, generally the superconducting proximity effect is not expected in insulators and particularly not in ferromagnetic insulators.

The situation may change in the presence of strong electric fields or under nonequilibrium conditions. For example, it is well known that a field $>10^7$ V/m can change the doping state of semiconductors via ionization, or breaking of electronic bonds, leading, respectively, to an avalanche, or Zener breakdown in *p-n* junctions. A variety of electric field effects has been reported in polarizable complex oxides,[30,31] including cuprates[32,33] and manganites.[34–42] In polar media the electric field can lead not only to charge transfer but also to structural changes[40–42] and electromigration, which cause resistive switching phenomena.[43] In FI manganites the electric field may depin immobile polarons, leading to a nonlinear electrical response at large bias voltage.[35,37] The nonlinear response at large bias is also inherent for tunnel

junctions with a thick insulating barrier. The electric field leads to a linear distortion of the tunnel barrier and facilitates Fowler-Nordheim type tunneling (field emission)[44] of hot electrons into the conduction band of the insulator. Such nonequilibrium electrons in the conduction band are mobile and in the case of a FI are fully spin polarized, which may lead to a significant change of magnetoresistance (MR) effects.[45]

In this paper we study the bias dependence of the perpendicular magnetotunneling characteristics of epitaxially grown nanoscale S/FI/S junctions made of the cuprate superconductor $YBa_2Cu_3O_{7-x}$ (YBCO) and the low-doped manganite $LaMnO_{3+\delta}$ (LMO) that is a ferromagnetic insulator below $T_{\mathrm{Curie}} \simeq 150$ K. It is observed that at low bias voltage the electron transport through the junctions is blocked due to the presence of the insulating band gap (polaronic mobility edge) and the lack of direct tunneling through the 20 nm thick LMO layer. However, at larger bias, $V > 0.3$ V, corresponding to the regime of Fowler-Nordheim tunneling into the conduction band of the insulator, excess current through the junction appears. Initially it increases gradually with increasing bias voltage, but at $V \sim 1$ V it jumps abruptly, leading to a steplike anomaly in the current-voltage characteristics. Such a steplike increase of the excess current exists only in the superconducting state and is easily suppressed by a magnetic field. The phenomenon is attributed to a different type of superconducting proximity effect of nonequilibrium electrons in the conduction band of the ferromagnetic insulator. The occurrence of this strongly nonequilibrium state in the LMO layer is confirmed by the direct detection of photon emission. Since the conduction band in our ferromagnetic insulator is fully spin polarized, the long range (20 nm) of the observed proximity effect points towards an unconventional spin-triplet superconducting state.

The paper is organized as follows. In Sec. II we describe the fabrication procedure of the YBCO/LMO heterostructures and the nanoscale YBCO/LMO/YBCO tunnel junctions. We demonstrate the reproducibility of the ferromagnetic and insulating properties of LMO layers both for a single layer and within YBCO/LMO multilayers with different layer thicknesses. In Sec. III we describe the perpendicular transport properties of the LMO layer in our junctions. It is shown that it undergoes a transition to the ferromagnetic insulator state at $T_{\mathrm{Curie}} \simeq 150$ K with a strongly bias-dependent CMR up to -600%. In Sec. IV we report the observation of a high bias anomaly in the junction characteristics, we demonstrate the occurrence of a Fowler-Nordheim tunneling into the conduction band of the FI, and we provide an interpretation of the anomaly in terms of a different type of superconducting proximity effect of nonequilibrium electrons in the conduction band of the ferromagnetic insulator. The presence of a strongly nonequilibrium electron and hole population in the conduction and valence bands of the FI is confirmed by the direct detection of photon emission from our junctions at large bias. Finally, we argue that the long range of the proximity effect through the FI indicates the unusual odd-spin-triplet nature of the superconducting order parameter. We also argue that the Fowler-Nordheim tunneling in the FI should lead to perfectly spin-polarized currents that are beneficial for spintronic applications.

II. SAMPLES

A. Fabrication and characterization of YBCO/LMO heterostructures

The YBCO/LMO heterostructures were deposited by pulsed laser deposition (PLD) on (001)-oriented $Sr_{0.7}La_{0.3}Al_{0.65}Ta_{0.35}O_3$ (LSAT) substrates similar as described in Ref. 46. The substrate temperature was 900 °C, the O_2 partial pressure 0.32 mbars, and the fluency and pulse frequency of the KrF 248 nm excimer laser were 2 J/cm^2 and 2 Hz, respectively. The growth dynamics was monitored with *in situ* reflection high-energy electron diffraction (RHEED) to ensure a two-dimensional growth mode with sharp interfaces between the individual layers. After the growth the sample was cooled to 700 °C at 10 °C/min where the oxygen pressure was increased to 1 bar. Subsequently, the sample was further cooled to 485 °C at a rate of 30 °C/min where it was annealed for 1 h before it was cooled to room temperature. Finally, the structures were covered by a protective gold layer (70 nm).

For comparison, we also grew single LMO layers on LSAT substrates. It is well known that the electronic and magnetic properties of these LMO films can be largely varied depending on the PLD growth conditions.[2] We studied extensively how these can be changed in a systematic way from an insulating and antiferromagnetic or glassy magnetic state, over an insulating ferromagnetic state to a metallic ferromagnetic state with a modification of the O_2 background gas pressure during PLD growth and a subsequent postannealing treatment in flowing oxygen or argon. This study, which will be presented in full length in a forthcoming publication, has established that the above mentioned growth conditions (an O_2 background pressure of 0.32 mbars and postannealing in flowing O_2 at 485 °C) yield LMO layers that are insulating and strongly ferromagnetic with a ferromagnetic moment of about $3\mu_B$ per Mn atom. The postannealing treatment does not strongly affect the FI properties of the LMO layer, but is required to fully oxygenate the YBCO layers as to achieve a sharp superconducting transition with a high critical temperature T_c.

The films were investigated with in-plane four-probe electric transport and magnetization measurements with a Quantum Design physical property measurement system (PPMS QD6000) with a vibrating sample magnetometer (VSM) option. To measure the high resistance of the single layer LMO films we used an external Keithley multimeter. The ellipsometry measurements were performed with a commercial rotating analyzer setup (Woollam VASE) in the range 0.5–6.5 eV and with a homebuilt one at 0.01–0.5 eV.[47] The substrate correction was performed with the commercial WVASE32 software package.

The FI properties of a 100 nm thick single LMO layer are demonstrated in Figs. 1(a)–1(c). The field-cooled magnetization data at 1 kOe in Fig. 1(a) show that a ferromagnetic state develops below $T_{\mathrm{Curie}} \simeq 160$ K with a sizable low temperature moment of about $2.8\mu_B$ per Mn ion. The insulating behavior is evident from the temperature dependence of the resistance shown in Fig. 1(b) as well as from the optical spectra in Fig. 1(c). The latter show a characteristic redistribution of spectral weight below T_{Curie} from high energies above 2 eV towards two low-energy bands that are peaked around 1.3 and

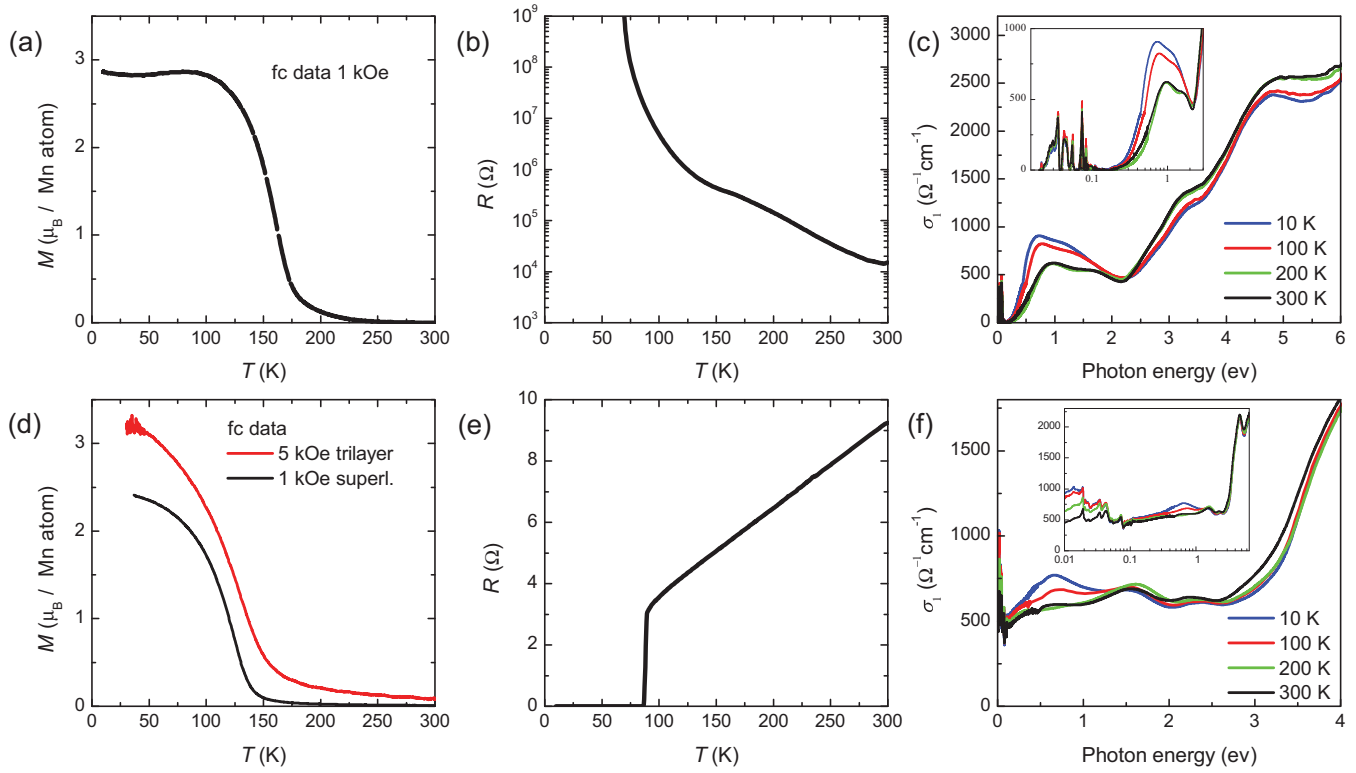

FIG. 1. (Color online) (a) Magnetization, (b) resistance, and (c) optical spectra of a single 100 nm thick LMO film showing its ferromagnetic insulator properties. (d) Field-cooled magnetization of a YBCO (10 nm)/LMO (10 nm)/YBCO (10 nm) trilayer at 5 kOe and a [YBCO (10 nm)/LMO (10 nm)] × 10 superlattice at 1 kOe. (e) Lateral resistance of the YBCO (10 nm)/LMO (10 nm)/YBCO (10 nm) trilayer with the contacts on the top YBCO layer. (f) Optical conductivity of the [YBCO (10 nm)/LMO (10 nm)] × 10 superlattice.

0.7 eV, respectively. A similar trend was previously reported for $La_{1.9}Sr_{0.1}MnO_3$ in the ferromagnetic insulating state[48] where the low-energy band was assigned to the response of strongly pinned polarons of orbital and/or magnetic origin.[4,5] The optical spectra and the resistivity data confirm that these polarons are strongly pinned and therefore do not contribute to a coherent charge transport. As shown in the inset, the peaks at low frequency are entirely due to infrared-active phonon modes. This is different from the ferromagnetic, metallic state of $La_{2/3}(Ca,Sr)_{1/3}MnO_3$ for which the spectral weight transfer from high to low energy gives rise to a pronounced Drude-like peak in the optical conductivity.

Figures 1(d)–1(f) demonstrate the reproducibility of the characteristics of YBCO/LMO multilayers with a different number of thin (10 nm) layers. It is seen that the thin LMO layers maintain their insulating ferromagnetic properties even if they are combined with YBCO in the form of YBCO/LMO multilayers. Figure 1(d) shows the temperature dependent magnetization of a YBCO (10 nm)/LMO (10 nm)/YBCO (10 nm) trilayer and a [YBCO (10 nm)/LMO (10 nm)] × 10 superlattice that were grown under similar conditions. They both reveal a ferromagnetic transition of the LMO layers at $T_{\mathrm{Curie}} \simeq 150$ K with a sizable magnetic moment of about $3\mu_B$ per Mn ion. Figure 1(e) shows the corresponding T dependence of the in-plane resistance for the unpatterned YBCO/LMO/YBCO trilayer. The in-plane resistance is dominated by the upper YBCO layer on which the contacts are placed and does not exhibit any noticeable contribution from the LMO layer that is situated underneath. The resistance exhibits a linear T dependence in the normal state and a sharp superconducting transition around $T_c \simeq 88$ K that is characteristic of the response of optimally doped YBCO. However, direct evidence that the LMO layers maintain their insulating properties in these YBCO/LMO multilayers has been obtained from the optical conductivity of a corresponding [YBCO (10 nm)/LMO (10 nm)] × 10 superlattice as shown in Fig. 1(f). The spectra also reveal the characteristic spectral weight redistribution from high energy above 1.5 eV towards a low-energy peak around 0.65 eV that occurs right below the ferromagnetic transition of the LMO layers at $T_{\mathrm{Curie}} \simeq 150$ K. Similar to the single LMO layer, for which the spectra are shown in Fig. 1(c), this low-energy peak can be assigned to the strongly pinned magnetopolarons. The additional Drude response which is present at all temperatures originates from the metallic YBCO layers.

B. Fabrication of 3D-nanosculptured YBCO/LMO/YBCO junctions

To study the perpendicular transport properties of the LMO layer, we fabricated small S/FI/S junctions using a three-dimensional (3D)-nanosculpturing technique.[49] The growth of the YBCO/LMO/YBCO (100/20/100 nm) heterostructure, covered by a protective Au layer (70 nm), was described in Sec. II A. This heterostructure was patterned into several ∼5 μm wide bridges using photolithography and cryogenic

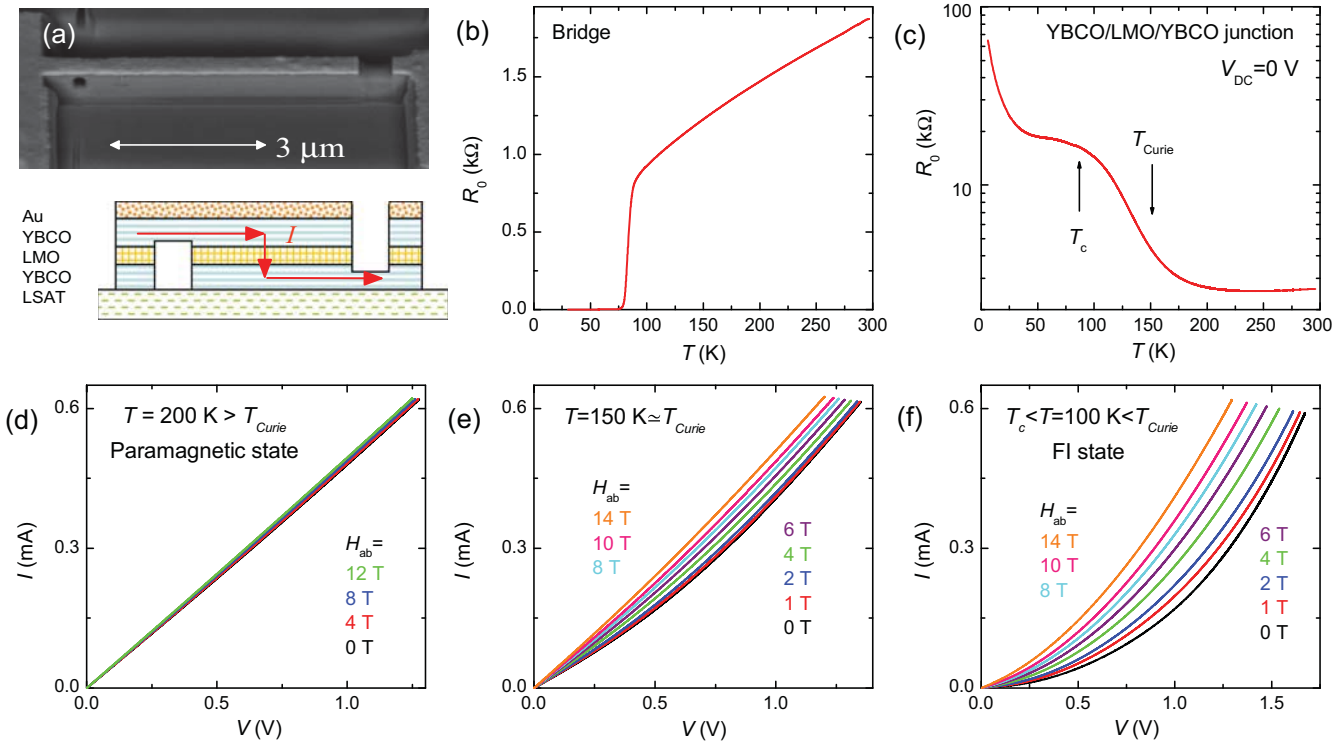

FIG. 2. (Color online) (a) Top panel: Scanning electron microscopy (SEM) image of a 3D-FIB patterned junction No. 2. Bottom panel: Side-view sketch of the structure (not in scale). Arrows indicate the current flow path. (b) In-plane resistive transition of the same bridge before the final FIB cut. A sharp superconducting transition occurs at $T_c \simeq 86$ K. (c) Temperature dependence of the out-of-plane zero-bias resistance $R_0(T)$ (in the semilogarithmic scale) of junction No. 2 at $H = 0$. The transition to the insulating behavior occurs at $T < T_{\rm Curie} \simeq 150$ K. Note that $R_0(T)$ reveals no sign of superconductivity at $T < T_c$, indicating the lack of a proximity effect at low bias. (d)–(f) Magnetic field dependence of the I-V curves of junction No. 4: (d) in the paramagnetic state $T = 200$ K, (f) close to the Curie temperature $T = 150\,\text{K} \simeq T_{\rm Curie}$, and (f) in the FI state $T = 100\,\text{K} < T_{\rm Curie}$. Negative colossal magnetoresistance appears in the FI state.

(liquid-nitrogen-cooled) reactive ion etching in an Ar plasma. At the next stage the central part of each bridge was narrowed to a submicron width using a focused ion beam (FIB), as shown in Fig. 2(a). Finally, two side cuts were made by FIB to interrupt the bottom YBCO and the top YBCO/Au layers. This leads to the appearance of a zigzag structure as sketched in the bottom part of Fig. 2(a). The arrow indicates the current flow path. The side cuts force the current to flow through the LMO layer, thus a small YBCO/LMO/YBCO (S/FI/S) tunnel junction is formed between the two side cuts. In total, three working junctions with similar characteristics were fabricated and studied.

Figure 2(b) shows the zero dc-bias (measured with small ac-bias current) in-plane resistive transition $R_0(T)$ of the 660 nm wide bridge (No. 2) in Fig. 2(a), before the final side cut through the top YBCO layer, but with an interrupted Au layer. A sharp superconducting transition at $T_c \simeq 86$ K is evident. A comparison with the superconducting transition for the unpatterned multilayer in Fig. 1(e) indicates that no significant deterioration of the YBCO layers has occurred during the patterning process. This is due to a low oxygen outdiffusion during cryogenic Ar-plasma etching and a sufficient thickness of the protective Au layer that prevents chemical passivation during the lithographic process and Ga implantation during FIB etching and viewing.

III. PERPENDICULAR TRANSPORT PROPERTIES OF THE LMO LAYER

In the following we present the transport measurements after the two side cuts were performed with the FIB to interrupt the bottom and top YBCO layers. Arrows in the bottom part of Fig. 2(a) indicate the current flow path in our junctions. The current is forced to flow across the LMO layer (in the c-axis direction) within the junction area. This allows direct probing of the perpendicular transport characteristics of the LMO layer inside the junctions.

A. Temperature dependence of the c-axis resistance of LMO

Figure 2(c) displays the temperature dependence of the zero-bias resistance $R_0(T)$ (measured with a small ac current) at zero applied magnetic field $H = 0$ for junction No. 2, as shown in Fig. 2(a). A comparison with the data for the same bridge before the final side cut through the top YBCO layer [Fig. 2(b)] reveals that the out-of-plane $R_0(T)$ of the junction differs both quantitatively and qualitatively from the in-plane $R_0(T)$ of the bridge. From room temperature to about 220 K the junction resistance decreases slightly with decreasing temperature. However, at $T < 150$ K the resistivity rapidly starts to increase with decreasing temperature, i.e., it shows an insulator-type behavior. At $T = 100$ K the resistance of the

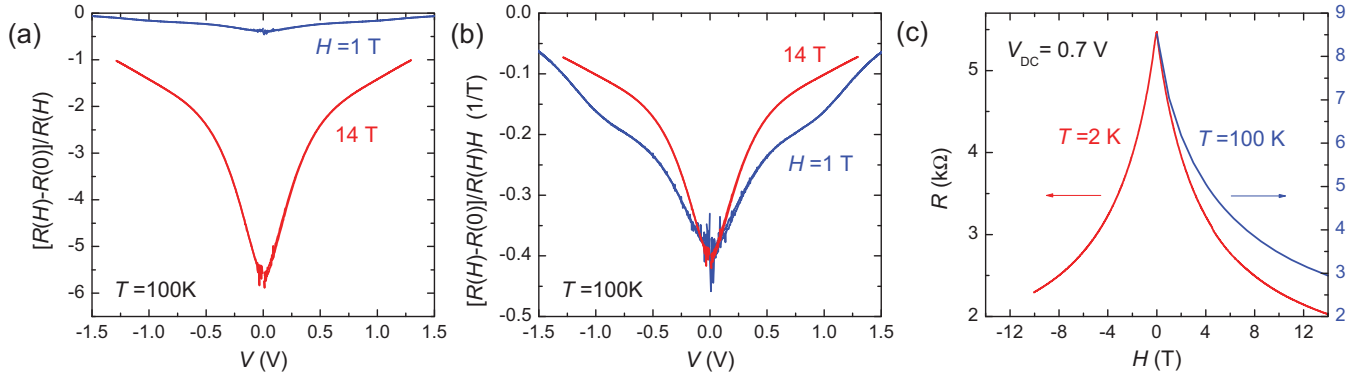

FIG. 3. (Color online) (a) Bias dependence of the magnetoresistance (MR) at in-plane fields of $H = 1$ and 14 T for junction No. 4. The MR reaches -600% at $H = 14$ T. (b) The same as in (a), normalized by the magnetic field. It is seen that at low bias $|V| < 0.1$ V the MR is approximately linear in field up to 14 T, at intermediate bias the MR is nonlinear in H, and it again becomes approximately linear at a higher bias $|V| \gtrsim 1.5$ V. (c) Nonlinear field dependence of the junction resistance at an intermediate bias $V = 0.7$ V at $T = 2$ (left axis) and 100 K (right axis).

junction is about 20 times larger than the one of the bridge. Although a minor drop of R_0 due to the superconducting transition of the YBCO electrodes is present, as marked by the upward arrow in Fig. 2(c), it is hardly visible on the scale of the plot. This demonstrates that the junction resistance at low temperatures is governed by the resistance of the LMO barrier. The c-axis resistivity of LMO at $T_c < T < T_{\rm Curie}$ with $\rho_c \sim 200$–$250\ \Omega$ cm is clearly nonmetallic. Therefore, the rapid upturn of $R_0(T)$ at $T < 150$ K indicates a transition of LMO into the insulating state. This temperature is similar to the Curie temperature of our single LMO film and coincides with $T_{\rm Curie}$ of LMO within the YBCO/LMO heterostructures as shown in Fig. 1. The resistance continues to rapidly increase at $T < 50$ K, showing a tendency for diverging at $T \to 0$, in a qualitative similarity with the behavior of the in-plane resistance of the single LMO film, shown in Fig. 1(b).

The comparison of Figs. 1(d) and 2(c) demonstrates that the upturn of $R_0(T)$ at $T < 150$ K follows the one of the magnetization. As shown below, it is also accompanied by the appearance of the colossal magnetoresistance, which is typical for ferromagnetic manganites. This proves that our LMO layer indeed enters the FI state below $T_{\rm Curie} \simeq 150$ K.

B. Bias dependence of the colossal magnetoresistance

The small area of our junctions allows the achievement of significant bias voltages at small currents and without significant self-heating.[50] This facilitates an accurate analysis of the genuine bias dependence of the perpendicular transport characteristics of LMO, without artifacts from self-heating.

Figures 2(d)–2(f) show the current-voltage (I-V) characteristics of junction No. 4 for different in-plane magnetic fields: (d) in the paramagnetic state at $T = 200$ K $> T_{\rm Curie}$, (e) close to the Curie temperature at $T = 150$ K, and (f) in the FI state at $T = 100$ K $< T_{\rm Curie}$. It is seen that in the paramagnetic state the I-V's are Ohmic and do not exhibit a significant MR. However, already at 150 K and even more so at 100 K, the I-V curves become nonlinear and exhibit a large negative MR.

Figure 3(a) shows the bias dependence of the magnetoresistance, $\mathrm{MR}(V) = [R(V,H) - R(V,0)]/R(V,H) = [1 - I(V,H)/I(V,0)]$, for junction No. 4 at $T = 100$ K for in-plane fields $H = 1$ and 14 T. At low bias the MR ($V \sim 0$) reaches -600% at $H = 14$ T, which is a clear signature of the CMR effect. With increasing bias the CMR rapidly decreases and falls to -100% at $V = 1.25$ V. The bias dependence of the MR at $V > 0.1$ V approximately follows the power law $\mathrm{MR}(V) \propto -|V|^{-0.7}$. Figure 3(b) shows the same data normalized by the magnetic field. It is seen that the field-normalized MR coincides both at low $|V| < 0.1$ V and high $|V| > 1.5$ V bias, but deviates at intermediate bias. This indicates that the MR at low and high bias is linear in field at least up to $H = 14$ T. However, the MR becomes significantly nonlinear at an intermediate bias of $V \sim 1$ V. This is demonstrated in Fig. 3(c), which shows the field dependence of the dc resistance $R = V/I$ at $V = 0.7$ V. The MR is isotropic with respect to field orientation, as shown in Fig. 4(a).

The observed bias dependence of the MR is similar to the one that was previously reported for magnetic tunnel junctions containing LMO layers.[13,51,52] The strong bias dependence is still not well understood because it may be caused by various intrinsic and extrinsic[53] mechanisms. Intrinsic mechanisms for the suppression of the MR at high bias can be due to inelastic spin-flip scattering of high-energy electrons,[54] or to a strong energy dependence of the electronic DOS near E_F.[8,55] Extrinsic reasons can be due to granularity and microscopic inhomogeneity of films,[51,53] or to oxygen variation at interfaces.[52]

Since our junctions contain only one magnetic layer, they are not of the spin-valve type. The epitaxial LMO layer is uniform in the c-axis direction at the scale of its thickness 20 nm. Therefore, it is unlikely that the observed strong bias dependence of the MR is of extrinsic origin, for example, due to a spin-valve effect that might occur in a granular structure. Rather, it is an intrinsic property of the LMO material. As described in Sec. IV C, the reduction of the MR at large bias is accompanied by a significant photon emission. This shows the occurrence of inelastic scattering in the LMO barrier and

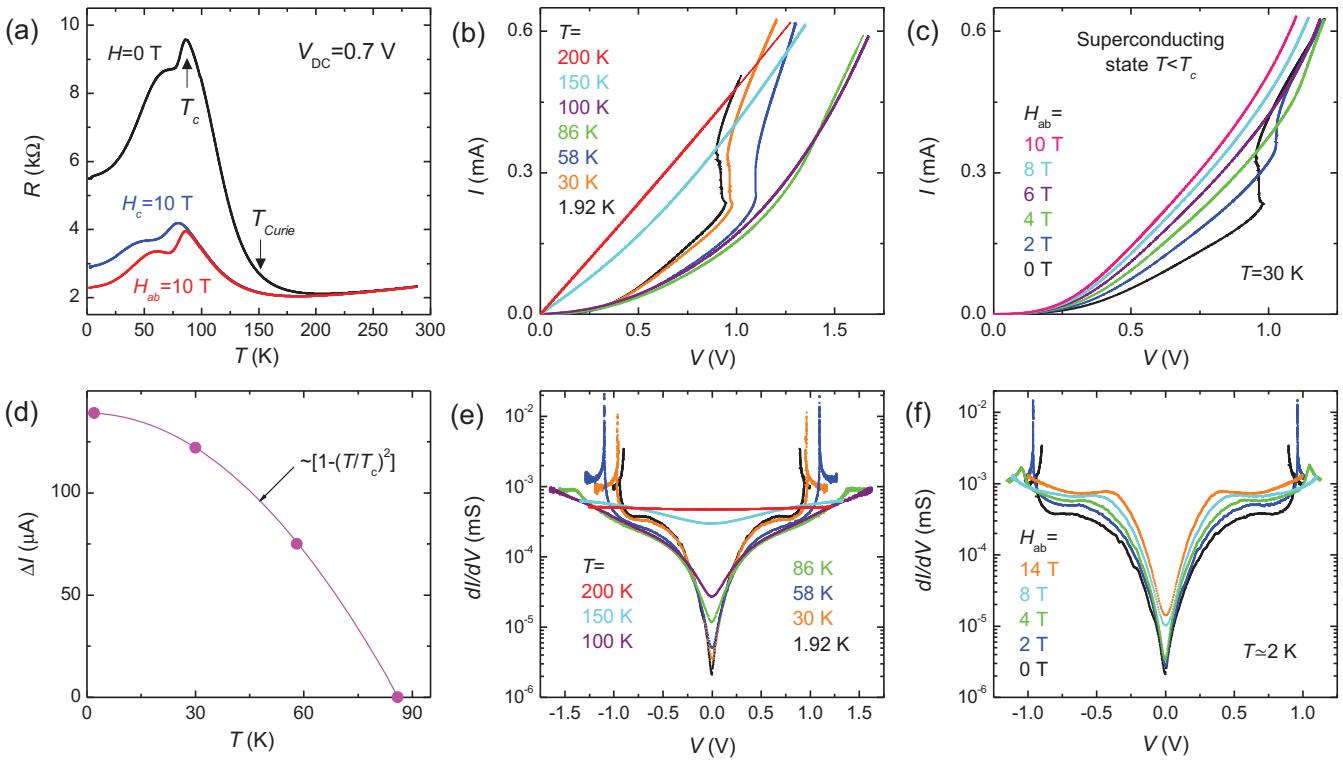

FIG. 4. (Color online) (a) Large bias dc resistance of junction No. 4 at $H = 0$ and 10 T applied along the ab plane and the c-axis direction. The upturn at $T < T_{\rm Curie} \sim 150$ K marks the transition to the FI state of LMO while the downturn at $T_c \simeq 86$ K indicates the appearance of a superconducting proximity effect. (b) I-V curves of junction No. 4 at different T and at $H = 0$. Below T_c, a steplike onset of excess current appears at a large bias voltage of about 1 V. (c) Magnetic field dependence of the I-V curves at $T = 30$ K. The steplike increase of the current is rapidly suppressed by a magnetic field. (d) T dependence of the excess current (step height) ΔI at high bias. (e) and (f) Differential conductance dI/dV of junction No. 4 (e) at different temperatures and $H = 0$, and (f) at different H and $T \simeq 2$ K.

points towards an intrinsic, spin-flip scattering mechanism[54] of the strong bias dependence of the CMR in LMO.

IV. TUNNELING CHARACTERISTICS OF YBCO/LMO/YBCO JUNCTIONS IN THE SUPERCONDUCTING STATE

Unlike the MR of LMO, the electronic and superconducting properties of the cuprates are strongly anisotropic. An out-of-plane magnetic field suppresses superconductivity due to the penetration of Abrikosov vortices.[56,57] However, an in-plane field of 10–17 T does not give rise to any visible suppression of superconductivity at $T \ll T_c$ [see, e.g., Fig. 3(d) in Ref. 56]. This is because the upper critical field H_{c2} of optimally doped cuprates is very high for the field parallel to ab planes. Therefore, to avoid complications with field screening and suppression of superconductivity in YBCO, in what follows we will focus on junction characteristics for in-plane magnetic fields that practically do not affect the YBCO electrodes.

Cooper pair tunneling in superconducting tunnel junctions should lead to the appearance of a Josephson supercurrent at $V = 0$. However, as seen from Fig. 2(c), the zero-bias resistance of the junction does not drop to zero at $T < T_c$. Instead, it continues to rapidly increase with decreasing T. Thus, there is no sign of a Josephson current at low bias. Our FI layers are too thick (20 nm) for the Cooper pair tunneling that is needed for achieving the Josephson coupling. Since the probability of Cooper pair and direct quasiparticle tunneling are the same, direct quasiparticle tunneling through the LMO layer in our junctions is also negligible.

A. High bias anomaly: Evidence for the superconducting proximity effect in LMO

Figure 4(a) shows the temperature dependence of the dc resistance at an intermediate bias of $V = 0.7$ V for junction No. 4 at $H = 0$ and 10 T parallel (ab plane) and perpendicular (c axis) to the film surface. It is seen that at $T > T_c$ the MR is isotropic with respect to the field orientation, which is typical for manganites. An anisotropy below T_c is caused by a partial screening of the perpendicular field by the superconducting YBCO layers. The comparison of Figs. 2(c) and 4(a) reveals a remarkable, qualitative difference in the temperature dependence of the junction resistances at low and high bias voltages in the superconducting state. At zero bias $R_0(T)$ grows monotonously with decreasing T, showing no sign of a Josephson coupling or superconducting proximity effect through the LMO layer. As was discussed above, this is expected since the LMO layer is insulating and too thick for direct tunneling. The absence of a proximity effect at low bias voltage proves that our junctions are free from microshots or extended nonmagnetic "dead" layers[19] at the S/F interfaces, in which a long-range superconducting proximity effect might be induced. This suggests that the very different behavior of

R_{dc} at higher bias voltages is an intrinsic effect due to the appearance of a superconducting proximity effect through the LMO layer.

Figure 4(b) shows the T evolution of the I-V curves for junction No. 4 at $H = 0$. It is seen that from 200 K down to $T_c \simeq 86$ K the resistance (voltage at a given current) increases with decreasing T. This leads to qualitatively similar insulating behavior at all bias levels at $T_c < T < T_{\rm Curie}$, as shown in Figs. 2(c) and 4(a). This trend is reversed at $T < T_c$ where the high bias resistance starts to decrease with decreasing T [compare the I-V curves at $T = 100, 86, 58, 30$, and 1.92 K in Fig. 4(b)], while the low bias resistance continues to increase with decreasing T, as seen from $R_0(T)$ in Fig. 2(c) and the dI/dV curves in Fig. 4(e). From Fig. 4(b) it is seen that the drop in R_{dc} is associated with the development of an excess current in the I-V curves at bias $V \gtrsim 0.3$ V. Initially the excess current increases monotonously with increasing V, but at high bias $V \sim 1$ V it jumps abruptly, leading to the appearance of a step in the I-V curves. The observed high bias anomaly resembles the sum-gap step in I-V's of SIS junctions,[56] but occurs at more than an order of magnitude larger voltage. Therefore, it is not related to the singularity in the quasiparticle DOS at the superconducting energy gap of the YBCO electrodes.[56,57] The observation and interpretation of this high bias anomaly at $T < T_c$ in these S/FI/S junctions is the central result of this work.

Figure 4(c) shows the magnetic field dependence of the I-V curves at $T = 30$ K. It is seen that the step is suppressed by the modest magnetic field, much smaller than the in-plane H_{c2} of YBCO. This resembles the behavior of Josephson current, which can be easily suppressed by magnetic field without suppression of superconductivity in electrodes.

From Fig. 4(b) it is seen that the step smears out and vanishes as the temperature increases and approaches T_c. Figure 4(d) shows the temperature dependence of the step amplitude ΔI. It follows a parabolic dependence $1 - (T/T_c)^2$ (solid curve) that is typical for the amplitude of the superconducting order parameter. As noted above, the most objective overview of bias, field, and T dependencies of junction characteristics is provided by the set of I-V's in Figs. 4(b) and 4(c). From those I-V's it is seen that the appearance of the excess current at $V > 0.3$ V, which causes the drop in large bias resistance at $T < T_c$ in Fig. 4(a), is related to the appearance of a steplike increment of current at $V \gtrsim 1$ V. Therefore, their simultaneous vanishing at $T > T_c$ is not coincidental, but rather a unanimous evidence that the excess current at large bias voltages is induced by superconductivity in YBCO electrodes.

Figures 4(e) and 4(f) show the T and H evolution of the differential conductance dI/dV curves (on a semilogarithmic scale) for the same junction. At low bias voltage they reveal a thermal-activation behavior, which can be recognized from the characteristic V shape of the dI/dV curves.[58] The well defined crossing point of the dI/dV curves at $V \simeq \pm 0.3$ V in Fig. 4(e) is indicative of an effective thermal activation energy of $U \simeq 0.3$ eV.[58] Notably, this is about half the value of the energy at which the polaronic band appears in the optical spectra in Figs. 1(c) and 1(f). Therefore, we ascribe $U \simeq 0.3$ eV to the polaronic mobility edge. At low T the current through the LMO barrier is blocked at low bias $eV < U$, as seen from the I-V curve in the inset of Fig. 5(a) (regime A). At intermediate bias (regime B) the I-V curve is nonlinear at $T < T_{\rm Curie}$ and the resistance drops at $T < T_c$, indicating the occurrence of the nontrivial long-range superconducting proximity effect

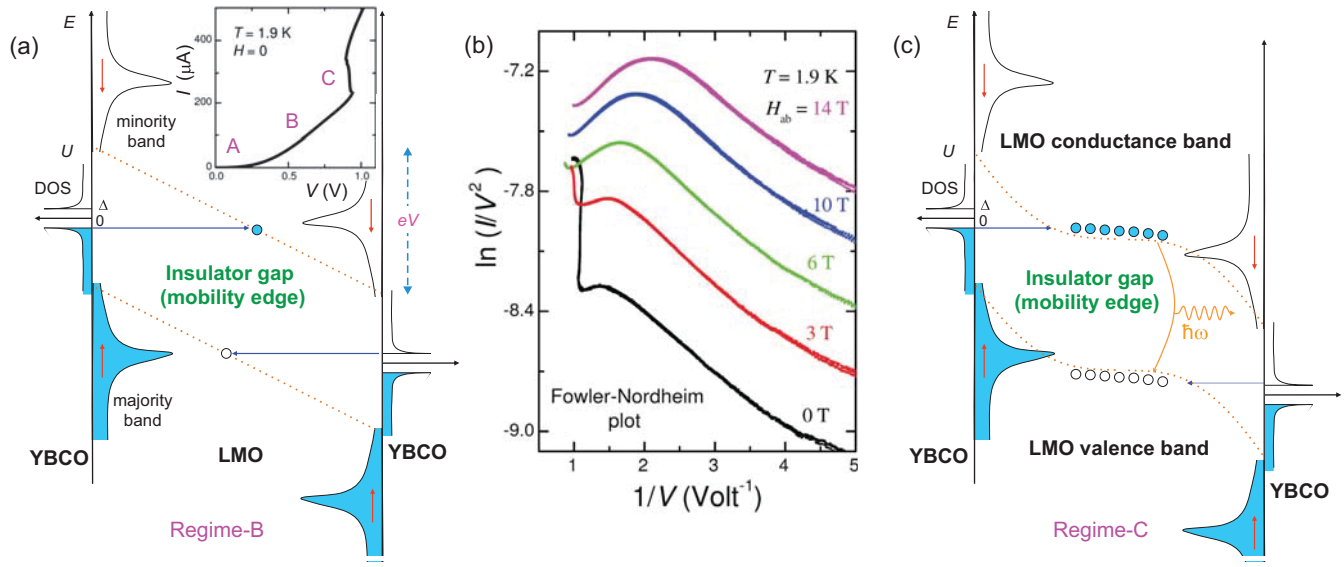

FIG. 5. (Color online) (a) Sketch of the tunneling diagram of our S/FI/S junctions. Horizontal arrows indicate Fowler-Nordheim type tunneling of electrons into the conduction band (minority spin ↓) and holes into the valence band (majority spin ↑) of LMO at $eV > U + \Delta$. Inset: I-V curve at $T = 1.9$ K showing that the current is blocked in regime A at $V \lesssim 0.3$ V. (b) Fowler-Nordheim plots for junction No. 4 at $T = 1.9$ K and different H. (c) Modified tunneling diagram with the proximity effect in the conduction and valence bands of LMO. The proximity effect leads to a reduction of the electric field in the central part of the LMO barrier and concentration near the interfaces. The shrinkage of the effective barrier width gives rise to an excess current.

through the ferromagnetic insulator. Finally, at high bias $V \gtrsim 1$ V (regime C) an excess current step appears at $T < T_c$.

B. Fowler-Nordheim tunneling into the conduction band of the LMO

To understand the origin of the steplike increase of the tunneling current, we sketch in Fig. 5(a) the tunneling diagram of our junctions: DOS versus energy and the coordinate across the junction. In YBCO there are singularities in the DOS at the superconducting gap energy of $\Delta \sim 30$ meV.[56,57] The electronic bands in LMO are spin polarized and are separated by the band gap (the polaronic mobility edge) $U \sim 0.3$ eV, corresponding to half the optical gap in Fig. 1(f), followed by maxima in the DOS at $E \sim 1$ eV.[1,6,59] The electric field is concentrated in the FI layer, which leads to the linear gradient of the electric potential, that is shown by the dotted lines.

Regime A: At low bias, $eV < U + \Delta \simeq 0.3$ V, electrons have to tunnel through the full thickness of the LMO layer. The probability of such a direct tunneling process is negligible due to the large thickness of the LMO layer (20 nm). This leads to the blocking of the tunnel current at $V \lesssim 0.3$ V that is seen from the dI/dV curves in Figs. 4(e) and 4(f) and the I-V curve in the inset of Fig. 5(a) (regime A).

Regime B: At intermediate bias, $0.3\ \text{V} < V < 1$ V, a Fowler-Nordheim type tunneling of electrons into the conduction band and holes into the valence band of the insulator becomes possible, as indicated by the two horizontal arrows (for electrons and holes) in Fig. 5(a). The reduction of the effective barrier thickness leads to a rapid increase of the tunnel current at $V \gtrsim 0.3$ V. Figure 5(b) represents the Fowler-Nordheim plot $\ln(I/V^2)$ vs $1/V$ for I-V's at different in-plane fields at $T = 1.9$ K. The broad straight parts are characteristic of Fowler-Nordheim tunneling through the triangular barrier.[44] The slope of the curves depends on the barrier height U. It is seen that it does not change with field, which is also seen from the field independence of the threshold voltages for dI/dV curves in Fig. 4(f).

Regime C: At $V \gtrsim 1$ V a step in I-V occurs. Since it does not return back at higher bias, the excess current is present at all bias voltages above the step. Figure 5(c) represents our interpretation of the unusual excess-current step. We assume that with increasing bias the Fowler-Nordheim tunneling leads to an enhancement of the nonequilibrium population of mobile electrons in the conduction band and holes in the valence band of LMO (beyond the polaronic mobility edge). Since the penetration of the superconducting wave function through the now much thinner triangular barrier is significant, such electrons acquire phase coherence with the YBCO electrodes via the proximity effect. This leads to a drop of the resistivity in the populated part of LMO, which in turn leads to a distortion of the electric potential, as shown by the dotted lines in Fig. 5(c). The electric field becomes small in the proximity-induced (central) part of the LMO, coaligned with the superconducting gap singularities of YBCO electrodes. To maintain the bias voltage, the electric field has to increase in the vicinity of the interfaces, which leads to a further shrinkage of the tunnel barrier and to an even larger increase of the current into the conduction band. Such a positive feedback leads to an instability, which shows up as a step in the I-V curve.

It should be mentioned that a similar steplike change of I-V curves at large bias has been reported for single manganite films and was attributed to either depinning of polarons,[35,37] or an acute Joule heating.[60] Joule heating can indeed cause artifacts in large area films due to large currents and dissipation powers. However, the step in I-V curves of our submicron junctions is not caused by self-heating. In general, self-heating becomes less significant in smaller structures (approximately linear with size).[50] From Fig. 4(b) it is seen that the power at the step is $\sim$0.3 mW, which, together with a realistic thermal resistance $\sim 10^4$ K/W, gives a modest heating of only several K. Most clearly, this is seen from the connection between the step amplitude ΔI and superconducting T_c in Fig. 4(d). If heating would be significantly higher, the step would vanish at a correspondingly lower temperature with respect to T_c.

The polaron depinning mechanism of high bias instability in LMO[35,37] can be relevant, provided that by the depinning one means that electrons become mobile if they are lifted by the energy U above E_F, which is equivalent to our discussion in terms of the conduction band in LMO. This scenario is not directly related to superconductivity. Indeed, the reminiscence of the step at $V \sim 1$ V can be seen even at $T = 100\ \text{K} > T_c$ in MR at $H = 1$ T in Fig. 3(b). However, in our case a well defined step in the I-V's is observed only in the superconducting state. We thus conclude that this type of the superconducting proximity effect in the conduction and valence bands of the ferromagnetic insulator greatly amplifies the phenomenon. This is also consistent with the observed suppression of the step by a modest in-plane magnetic field of $H = 6$ T in Fig. 4(c). This field is much smaller than the in-plane H_{c2} and does not significantly affect superconductivity in the YBCO electrodes.[56] However, it is sufficient for suppression of the weak, proximity-induced phase coherence in the LMO layer, similar to that observed for the conventional proximity effect in S/N multilayers.[61]

Note that we do not assume the establishment of Josephson coupling, i.e., the appearance of the true supercurrent, through the junction. Rather we assume that the phase coherence is only partial with one of the electrodes. Namely, for the case of Fig. 5(c), nonequilibrium electrons in the conduction band acquire phase coherence only with the left electrode, in which the Fermi level is coaligned with the band edge. The situation is similar to the case of proximity-induced excess conductance in a superconductor-insulator-normal metal (SIN) structure. The appearance of such an excess conductance in LMO leads to the distortion of the electric field and triggers the discussed instability in the I-V curve caused by the concentration of the electric field and enhancement of the Fowler-Nordheim tunneling.

C. Light emission at the step: Evidence for the strong nonequilibrium population in LMO

The proposed scenario suggests the presence of a strongly nonequilibrium electron and hole population in the conduction and valence bands of LMO, respectively. The subsequent electron-hole recombination should be accompanied by an inelastic emission of bosons with an energy of $2U \sim 0.6$ eV, as indicated by the dotted curves in Fig. 5(c). The occurrence of photon[62] or phonon[63] emission upon inelastic tunneling

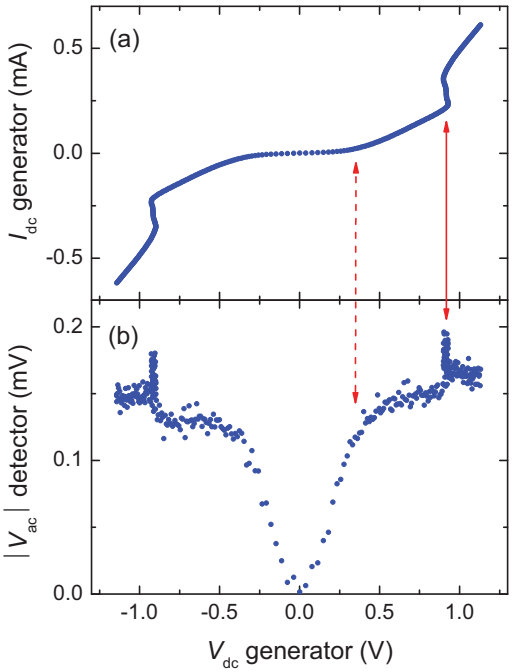

FIG. 6. (Color online) Radiation detection from junction No. 4 at $T = 1.8$ K and $H = 0$. (a) The I-V of the generator junction No. 4. (b) The signal of the detector junction. The appearance of a significant photon emission above the polaronic mobility edge in LMO (dashed line) and resonant enhancement of emission at the step (solid line) are seen.

is a well known phenomenon. To check the presence of the emission, we employed another junction on the same chip as a radiation detector. This detector junction was physically separated and electrically disconnected from the generator junction to ensure that only photons, propagating through the open space, can be detected. The generator junction was biased with a slowly sweeping dc voltage and a superimposed small ac modulation. The latter plays the role of a chopper and modulates the radiation power at the detector. The detector junction was biased at a constant dc voltage of 0.5 V, slightly above the polaronic mobility edge. The detection occurs via photon assisted tunneling: Absorbed photons create nonequilibrium hot electrons and cause excess current through the detector junction.

Figure 6(b) shows the absolute value of the first harmonics (chopper) signal from the detector as a function of the dc voltage at the generator. It is clearly seen that the emission starts above the polaronic mobility edge in LMO at $V \gtrsim 0.3$ V (dashed arrow in Fig. 6). At the step a pronounced emission enhancement takes place, as marked by the solid arrow in Fig. 6. Since relaxation of nonequilibrium quasiparticles in a superconductor is typically accompanied by the generation of phonons, rather than photons,[64] the observation of a significant photon emission supports our interpretation that inelastic processes are taking place in the LMO layer.

V. CONCLUSIONS

To conclude, we have studied small all-perovskite S/FI/S tunnel junctions made from epitaxially grown YBCO/LMO/YBCO heterostructures by 3D nanosculpturing. We observed a steplike enhancement of the current through the junction at a high bias of $V \sim 1$ V that was ascribed to a different type of superconducting proximity effect due to nonequilibrium electrons and holes that are injected in the conduction and valence bands of the ferromagnetic insulator via Fowler-Nordheim tunneling.

Since LMO is a FI with strongly spin-polarized conduction (minority) and valence (majority) bands, the observed long-range proximity effect across the 20 nm thick LMO layer is indicative of an unconventional spin-triplet component of the superconducting order parameter. Such a long-range proximity effect through a 20 nm thick FI layer is certainly not expected for the conventional spin-singlet SC order parameter of the cuprate high T_c superconductors. As discussed in Refs. 17 and 18, the transformation to a so-called odd-frequency spin-triplet order parameter requires a spin-active interface with a noncollinear magnetic order. A modulation of the ferromagnetic order at the YBCO/manganite interface has indeed been reported in Refs. 65–69 and may trigger such a transformation. The suggestion of a spin-triplet nature of the observed long-range proximity effect in our insulating LMO is in accord with similar reports for half-metallic manganites.[24–27]

Fowler-Nordheim tunneling through the conduction and valence bands of the FI should be fully spin polarized. Therefore, we anticipate that such YBCO/LMO/YBCO junctions may act as ideal spin-filter devices for spintronic applications.[8,13] Interestingly, spin segregation should occur in the structure. As indicated in Fig. 5(a), ↑ electrons should be accumulated in both YBCO films (only ↓ electrons leave the left YBCO and only ↑ electrons arrive at the right YBCO electrode). Consequently, ↓ electrons are accumulated in LMO.

The observation of resonant enhancement of light emission at the step in the I-V at $T < T_c$ [Fig. 6(b)] is consistent with similar reports in superconductor/semiconductor/superconductor light emitting diodes.[70] The enhancement of light emission can be attributed either to pairwise electron-hole recombination in the presence of Cooper pairing,[70] or to the establishment of Josephson-like phase coherence across the structure upon emission of the photon, satisfying the ac-Josephson relation, which may even lead to lasing at high bias.[71]

Finally we note that the practical applications of complex oxides is often hindered by various materials issues. In this respect it is important to emphasize the very good stability of our samples. No visible deterioration was detected over a 1 yr period at atmospheric conditions. This indicates a very good crystalline and chemical matching between YBCO and LMO, which facilitates the fabrication of high-quality epitaxial heterostructures for the use in fully spin-polarized spintronic components.

ACKNOWLEDGMENTS

We are grateful to Ya. Fominov for valuable remarks. Support by the Swedish Research Council, the SU-Core facility in Nanotechnology, the SNF Grants No. 200020-129484 and No. 200020-140225, and the NCCR MaNEP is gratefully acknowledged.

*vladimir.krasnov@fysik.su.se
†Present address: Department of Physics, Indian Institute of Technology Madras, 600 036 Chennai, India.

[1] J. M. D. Coey, M. Viret, and S. von Molnar, Adv. Phys. **48**, 167 (1999).
[2] W. S. Choi, Z. Marton, S. Y. Jang, S. J. Moon, B. C. Jeon, J. H. Shin, S. S. A. Seo, T. W. Noh, K. Myung-Whun, H. N. Lee, and Y. S. Lee, J. Phys. D: Appl. Phys. **42**, 165401 (2009); H. S. Kim and H. M. Christen, J. Phys.: Condens. Matter **22**, 146007 (2010).
[3] A. J. Millis, B. I. Shraiman, and R. Mueller, Phys. Rev. Lett. **77**, 175 (1996).
[4] J. Geck, P. Wochner, S. Kiele, R. Klingeler, A. Revcolevschi, M. V. Zimmermann, B. Büchner, and P. Reutler, New J. Phys. **6**, 152 (2004).
[5] R. Kilian and G. Khaliullin, Phys. Rev. B **60**, 13458 (1999).
[6] S. Seiro, Y. Fasano, I. Maggio-Aprile, E. Koller, O. Kuffer, and Ø. Fischer, Phys. Rev. B **77**, 020407(R) (2008).
[7] L. E. Hueso, J. M. Pruneda, V. Ferrari, G. Burnell, J. P. Valdés-Herrera, B. D. Simons, P. B. Littlewood, E. Artacho, A. Fert, and N. D. Mathur, Nature (London) **445**, 410 (2007).
[8] G.-X. Miao, M. Münzenberg, and J. S. Moodera, Rep. Prog. Phys. **74**, 036501 (2011).
[9] S. Sahoo, T. Kontos, J. Furer, Ch. Hoffmann, M. Gräber, A. Cottet, and Ch. Schönenberger, Nat. Phys. **1**, 99 (2005).
[10] S. Yuasa, T. Nagahama, and Y. Suzuki, Science **297**, 234 (2002).
[11] T. Niizeki, N. Tezuka, and K. Inomata, Phys. Rev. Lett. **100**, 047207 (2008).
[12] X. Zhang, B. Z. Li, G. Sun, and F. C. Pu, Phys. Rev. B **56**, 5484 (1997).
[13] U. Lüders, M. Bibes, S. Fusil, K. Bouzehouane, E. Jacquet, C. B. Sommers, J.-P. Contour, J.-F. Bobo, A. Barthélémy, A. Fert, and P. M. Levy, Phys. Rev. B **76**, 134412 (2007).
[14] R. Meservey and P. M. Tedrow, Phys. Rep. **4**, 173 (1994).
[15] K. Senapati, M. G. Blamire, and Z. H. Barber, Nat. Mater. **10**, 849 (2011).
[16] A. I. Buzdin, Rev. Mod. Phys. **77**, 935 (2005).
[17] F. S. Bergeret, A. F. Volkov, and K. B. Efetov, Rev. Mod. Phys. **77**, 1321 (2005).
[18] Y. Asano, Y. Sawa, Y. Tanaka, and A. A. Golubov, Phys. Rev. B **76**, 224525 (2007).
[19] V. A. Oboznov, V. V. Bolginov, A. K. Feofanov, V. V. Ryazanov, and A. I. Buzdin, Phys. Rev. Lett. **96**, 197003 (2006).
[20] I. Sosnin, H. Cho, V. T. Petrashov, and A. F. Volkov, Phys. Rev. Lett. **96**, 157002 (2006).
[21] J. W. Robinson, J. D. S. Witt, and M. G. Blamire, Science **329**, 59 (2010).
[22] T. S. Khaire, M. A. Khasawneh, W. P. Pratt, Jr., and N. O. Birge, Phys. Rev. Lett. **104**, 137002 (2010).
[23] R. S. Keizer, S. T. B. Goennenwein, T. M. Klapwijk, G. Miao, G. Xiao, and A. Gupta, Nature (London) **439**, 825 (2006).
[24] T. Hu, H. Xiao, C. Visani, Z. Sefrioui, J. Santamaria, and C. C. Almasan, Phys. Rev. B **80**, 060506(R) (2009).
[25] K. Dybko, K. Werner-Malento, P. Aleshkevych, M. Wojcik, M. Sawicki, and P. Przyslupski, Phys. Rev. B **80**, 144504 (2009).
[26] Y. Kalcheim, T. Kirzhner, G. Koren, and O. Millo, Phys. Rev. B **83**, 064510 (2011).
[27] C. Visani, Z. Sefrioui, J. Tornos, C. Leon, J. Briatico, M. Bibes, A. Barthelemy, J. Santamaria, and J. E. Villegas, Nat. Phys. **8**, 539 (2012).
[28] S. Kawabata and Y. Asano, J. Low Temp. Phys. **36**, 915 (2010); S. Kawabata, Y. Tanaka, A. A. Golubov, A. S. Vasenko, and Y. Asano, J. Magn. Magn. Mater. **324**, 3467 (2012).
[29] M. Fogelström, Phys. Rev. B **62**, 11812 (2000).
[30] K. Ueno, S. Nakamura, H. Shimotani, A. Ohtomo, N. Kimura, T. Nojima, H. Aoki, Y. Iwasa, and M. Kawasaki, Nat. Mater. **7**, 855 (2008).
[31] C. H. Ahn, A. Bhattacharya, M. Di Ventra, J. N. Eckstein, C. Daniel, M. E. Gershenson, A. M. Goldman, I. H. Inoue, J. Mannhart, A. J. Millis, A. F. Morpurgo, D. Natelson, and J.-M. Triscone, Rev. Mod. Phys. **78**, 1185 (2006).
[32] Y. Koval, X. Jin, Ch. Bergmann, Y. Simsek, L. Özyüzer, Paul Müller, H. Wang, G. Behr, and B. Büchner, Appl. Phys. Lett. **96**, 082507 (2010).
[33] H. Motzkau, Th. Jacobs, S. O. Katterwe, A. Rydh, and V. M. Krasnov, Phys. Rev. B **85**, 144519 (2012).
[34] A. Asamitsu, Y. Tomioka, H. Kuwahara, and Y. Tokura, Nature (London) **388**, 50 (1997).
[35] C. N. R. Rao, A. R. Raju, V. Ponnambalam, S. Parashar, and N. Kumar, Phys. Rev. B **61**, 594 (2000).
[36] S. Srivastava, N. K. Pandey, P. Padhan, and R. C. Budhani, Phys. Rev. B **62**, 13868 (2000).
[37] A. Wahl, S. Mercone, A. Pautrat, M. Pollet, Ch. Simon, and D. Sedmidubsky, Phys. Rev. B **68**, 094429 (2003).
[38] Y. Q. Ma, W. H. Song, J. M. Dai, R. L. Zhang, J. Yang, B. C. Zhao, Z. G. Sheng, W. J. Lu, J. J. Du, and Y. P. Sun, Phys. Rev. B **70**, 054413 (2004).
[39] F. X. Hu, J. Gao, and X. S. Wu, Phys. Rev. B **72**, 064428 (2005).
[40] Y. Murakami, S. Konno, T. Arima, D. Shindo, and T. Suzuki, Phys. Rev. B **81**, 140102 (2010).
[41] J. O. Krisponeit, C. Kalkert, B. Damaschke, V. Moshnyaga, and K. Samwer, Phys. Rev. B **82**, 144440 (2010).
[42] P. Mondal, D. Bhattacharya, and P. Mandal, Phys. Rev. B **84**, 075111 (2011).
[43] R. Waser and M. Aono, Nat. Mater. **6**, 833 (2007).
[44] R. G. Forbes, J. Appl. Phys. **103**, 114911 (2008).
[45] T. Nagahama, T. S. Santos, and J. S. Moodera, Phys. Rev. Lett. **99**, 016602 (2007).
[46] V. K. Malik *et al.*, Phys. Rev. B **85**, 054514 (2012).
[47] C. Bernhard, J. Humlicek, and B. Keimer, Thin Solid Films **455**, 143 (2004).
[48] Y. Okimoto, T. Katsufuji, T. Ishikawa, T. Arima, and Y. Tokura, Phys. Rev. B **55**, 4206 (1997).
[49] T. Golod, A. Rydh, and V. M. Krasnov, Phys. Rev. Lett. **104**, 227003 (2010).
[50] V. M. Krasnov, A. Yurgens, D. Winkler, and P. Delsing, J. Appl. Phys. **89**, 5578 (2001).
[51] J. Z. Sun, D. W. Abraham, K. Roche, and S. S. P. Parkin, Appl. Phys. Lett. **73**, 1008 (1998).
[52] J. Hayakawa, K. Ito, S. Kokado, M. Ichimura, A. Sakuma, M. Sugiyama, H. Asano, and M. Matsui, J. Appl. Phys. **91**, 8792 (2002).
[53] M. Ziese, Rep. Prog. Phys. **65**, 143 (2002).
[54] D. C. Tsui, R. E. Dietz, and L. R. Walker, Phys. Rev. Lett. **27**, 1729 (1971).
[55] S. Mukhopadhyay, I. Das, S. P. Pai, and P. Raychaudhuri, Appl. Phys. Lett. **86**, 152108 (2005).
[56] V. M. Krasnov, H. Motzkau, T. Golod, A. Rydh, S. O. Katterwe, and A. B. Kulakov, Phys. Rev. B. **84**, 054516 (2011).

[57] I. Maggio-Aprile, Ch. Renner, A. Erb, E. Walker, and Ø. Fischer, Phys. Rev. Lett. **75**, 2754 (1995).
[58] S. O. Katterwe, A. Rydh, and V. M. Krasnov, Phys. Rev. Lett. **101**, 087003 (2008).
[59] C. R. Hughes, J. Shi, A. D. Beyer, and N.-C. Yeh, Phys. Rev. B **82**, 134441 (2010).
[60] A. Palanisami, M. B. Weissman, and N. D. Mathur, Phys. Rev. B **71**, 094419 (2005); S. Mercone, R. Fresard, V. Caignaert, C. Martin, D. Saurel, C. Simon, G. Andre, P. Monod, and F. Fauth, J. Appl. Phys. **98**, 023911 (2005); Y. F. Chen and M. Ziese, *ibid*. **101**, 103902 (2007); A. A. Wagh, P. S. A. Kumar, H. L. Bhat, and S. Elizabeth, *ibid*. **108**, 063703 (2010).
[61] V. M. Krasnov, A. E. Kovalev, V. A. Oboznov, and N. F. Pedersen, Phys. Rev. B **54**, 15448 (1996).
[62] J. Lambe and S. L. McCarthy, Phys. Rev. Lett. **37**, 923 (1974).
[63] S. O. Katterwe, H. Motzkau, A. Rydh, and V. M. Krasnov, Phys. Rev. B **83**, 100510(R) (2011).
[64] V. M. Krasnov, Phys. Rev. Lett. **103**, 227002 (2009).
[65] J. Stahn, J. Chakhalian, Ch. Niedermayer, J. Hoppler, T. Gutberlet, J. Voigt, F. Treubel, H-U. Habermeier, G. Cristiani, B. Keimer, and C. Bernhard, Phys. Rev. B **71**, 140509(R) (2005).
[66] J. Chakhalian, J. W. Freeland, G. Srajer, J. Strempfer, G. Khaliullin, J. C. Cezar, T. Charlton, R. Dalgliesh, C. Bernhard, G. Cristiani, H.-U. Habermeier, and B. Keimer, Nat. Phys. **2**, 244 (2006).
[67] J. Hoppler, J. Stahn, Ch. Niedermayer, V. K. Malik, H. Bouyanfif, A. J. Drew, M. Rössle, A. Buzdin, G. Cristiani, H.-U. Habermeier, B. Keimer, and C. Bernhard, Nat. Mater. **8**, 315 (2009).
[68] R. Werner, C. Raisch, A. Ruosi, B. A. Davidson, P. Nagel, M. Merz, S. Schuppler, M. Glaser, J. Fujii, T. Chassé, R. Kleiner, and D. Koelle, Phys. Rev. B **82**, 224509 (2010).
[69] D. K. Satapathy *et al*., Phys. Rev. Lett. **108**, 197201 (2012).
[70] I. Suemune, H. Sasakura, Y. Hayashi, K. Tanaka, T. Akazaki, Y. Asano, R. Inoue, H. Takayanagi, E. Hanamura, J.-H. Huh, C. Hermannstädter, S. Odashima, and H. Kumano, Jpn. J. Appl. Phys. **51**, 010114 (2012).
[71] F. Godschalk, F. Hassler, and Y. V. Nazarov, Phys. Rev. Lett. **107**, 073901 (2011).